To protect the rights of the author(s) and publisher we inform you that this PDF is an uncorrected proof for internal business use only by the author(s), editor(s), reviewer(s), Elsevier and typesetter SPi. It is not allowed to publish this proof online or in print. This proof copy is the copyright property of the publisher and is confidential until formal publication.

AUTHOR QUERY FORM

ELSEVIER	**Book: Numerical modelling of failure in advanced composite materials Chapter: 12**	**Please e-mail your responses and any corrections to: E-mail: S.Kabilan@spi-global.com**

Dear Author,

Any queries or remarks that have arisen during the processing of your manuscript are listed below and are highlighted by flags in the proof. (AU indicates author queries; ED indicates editor queries; and TS/TY indicates typesetter queries.) Please check your proof carefully and answer all AU queries. Mark all corrections and query answers at the appropriate place in the proof using on-screen annotation in the PDF file. For a written tutorial on how to annotate PDFs, click http://www.elsevier.com/__data/assets/pdf_file/0016/203560/Annotating-PDFs-Adobe-Reader-9-X-or-XI.pdf. A video tutorial is also available at http://www.screencast.com/t/9OIDFhihgE9a. Alternatively, you may compile them in a separate list and tick off below to indicate that you have answered the query.

Please return your input as instructed by the project manager.

Location in Chapter	**Query / remark**
AU:1, page 334	Please check the inserted citation of Figure 12.2.

To protect the rights of the author(s) and publisher we inform you that this PDF is an uncorrected proof for internal business use only by the author(s), editor(s), reviewer(s), Elsevier and typesetter SPi. It is not allowed to publish this proof online or in print. This proof copy is the copyright property of the publisher and is confidential until formal publication.

c0005 # Peridynamics for analysis of failure in advanced composite materials

12

*A. Askari**, *Y. Azdoud*†, *F. Han*†, *G. Lubineau*†, *S. Silling*‡
*Boeing Commercial Airplane, Everett, WA, USA, †King Abdullah University of Science and Technology (KAUST), Thuwal, Saudi Arabia, ‡Sandia National Laboratories, Albuquerque, NM, USA

s0010 ## 12.1 Introduction

p0010 Many mathematical models and computational methods have been proposed and developed to predict the evolution of degradation in composites (Soden et al., 1998; Hinton et al., 2002; Lubineau and Ladevèze, 2008). However, predicting the behavior up to failure of these materials using conventional continuum damage mechanics or fracture mechanics remains challenging.

p0015 On the one hand, anisotropic damage mechanics has been adapted for composite materials, and it has reached a level where it can describe every single classical mechanism in laminates (Lubineau and Ladevèze, 2008). For example, the damage mesomodel for laminates (Ladevèze and Le Dantec, 1992), coupled with micro- and mesomechanics since the last decade (Ladevèze and Lubineau, 2001, 2003; Ladevèze et al., 2006), can predict in an accurate manner the progressive evolution of transverse cracking, diffuse damage (fiber/matrix debonding), interlaminar plasticity, fiber breaking, as well as interlaminar delamination. Yet, handling the final localization (which is key because it results in macroscopic cracks and failure) is somehow challenging as specific techniques have to be used (Allix and Deu, 1997; Allix et al., 2003) to ensure mesh objectivity, which remains not yet completely understood for laminated composites. We also note that damage mechanics-based approaches do not allow (at least in their raw formulation) for discontinuous solutions. Cracks are smoothed out and globally represented by internal damage variables. This is relevant to progressive and distributed degradation, but might be questioned as relevant to the final failure that generally results from the severe localization of a macroscopic crack, which shifts the failure to a regime in which homogenization may not be possible.

p0020 On the other hand, fracture mechanics mainly addresses the extension of preexisting cracks and does not address the initiation problem that is quite complex, especially in laminated composites. Even predicting crack extension is somewhat difficult when multiple cracks with complex shapes and interactions have to be considered, as a remeshing process is often needed if the finite element framework is used. Although remeshing can be avoided with some special elements, such as cohesive elements, a priori knowledge of the crack path is required to place these elements (Kilic et al., 2009). Placing the elements is generally possible for a limited number of configurations, such as the

Numerical modelling of failure in advanced composite materials. http://dx.doi.org/10.1016/B978-0-08-100332-9.00012-8
© 2015 Elsevier Inc. All rights reserved.

Comp. by: KKalaiselvi Stage: Proof Chapter No.: 12 Title Name: Camanho
Date:23/4/15 Time:13:18:57 Page Number: 331

To protect the rights of the author(s) and publisher we inform you that this PDF is an uncorrected proof for internal business use only by the author(s), editor(s), reviewer(s), Elsevier and typesetter SPi. It is not allowed to publish this proof online or in print. This proof copy is the copyright property of the publisher and is confidential until formal publication.

prediction of interlaminar delamination, in which cracks clearly appear and extend at the interface between adjacent plies (Allix and Ladevèze, 1995). Nevertheless, location of cracks is usually unknown a priori in complex structures. Similarly, prediction of crack propagations also requires an additional growth criterion. This criterion is a priori based on material properties and local loading conditions. However, it is extremely difficult to identify such a criterion for cracks propagation from experimental data, especially in composite materials.

p0025 To address these concerns, a recently developed theory of solid mechanics, known as peridynamics and proposed by Silling (2000), redefines the problem by using integral equations rather than partial differential equations. In peridynamics, the equilibrium of a material point is assumed to be attained by an integral of internal forces exerted by nonadjacent points across a finite distance. These internal forces are thus nonlocal interactions in a continuous body. The interaction between pairs of points is defined over the connection vector, called the *bond*, of these two points. A bond is permitted to break irreversibly when it is stretched beyond a critical value. As a result, two-dimensional surfaces crossing all broken bonds represent cracks in a three-dimensional body. These definitions allow crack initiation and evolution simultaneously at multiple sites, with spontaneous paths inside a material and without formulating a complex crack growth criterion (Kilic et al., 2009).

p0030 Peridynamics, however, comes with huge computational cost that pushes classical engineering problems out of reach. Furthermore, peridynamics is characterized by volume like boundary conditions that can make its application tedious for engineers who are more used to traction like boundary conditions. Consequently, a reasonable strategy is to reserve peridynamics for parts of the structure where key mechanisms, such as damage or fracture, strongly impact the solution, and then to use continuum mechanics for the rest of the structure for which the conventional continuum model can satisfy solution accuracy and boundary conditions and can reduce consumption of computational resources. Then, the challenge lies in how to couple the peridynamic model and the conventional continuum model together efficiently. Recently, some coupling schemes have been proposed, including the force-based coupling method (Seleson et al., 2013), the Arlequin coupling method (Han and Lubineau, 2012) and the morphing coupling method (Lubineau et al., 2012). The force-based coupling method derives a coupled force equilibrium equation, which blends the peridynamic and continuum models in a transition region by using a weighting function. In contrast, the Arlequin coupling method belongs to the energy-based coupling strategy in which the coupling is performed at the energy level by using a partition of unity concept. The morphing coupling method is inspired by the idea of homogenization. Using the equivalent energy density of both models, it constructs a balance between local stiffness and the weighted nonlocal modulus.

p0035 In the remainder of this chapter, Section 12.2 briefly introduces the fundamentals of peridynamic theory. Special peridynamic material models for composites are addressed in Section 12.3. As a very recent method to formalize continuum mechanics reference problems, peridynamics is still at its infancy when it comes to complex material behaviors such as those observed in laminated composites. Even so, we provide a few examples based on our recent work and discuss needed developments and

Comp. by: KKalaiselvi Stage: Proof Chapter No.: 12 Title Name: Camanho
Date:23/4/15 Time:13:18:57 Page Number: 332

To protect the rights of the author(s) and publisher we inform you that this PDF is an uncorrected proof for internal business use only by the author(s), editor(s), reviewer(s), Elsevier and typesetter SPi. It is not allowed to publish this proof online or in print. This proof copy is the copyright property of the publisher and is confidential until formal publication.

B978-0-08-100332-9.00012-8, 00012

the potential of the approach. We then focus on the upscaling problem and on how to handle the simulation of large structures by restricting the use of peridynamics to localized areas. Because the morphing coupling method is simple and easy to use, we present a brief introduction on this method and provide a benchmark example for crack extension in Section 12.4.

s0015 12.2 Peridynamic theory

p0040 Peridynamic theory is a generalization of standard solid mechanics that is adapted to certain applications in which the standard theory either fails to apply or requires extensive modification. In particular, peridynamics applies to the modeling of defects, especially cracks, that form spontaneously and grow. To accomplish this, peridynamic equations omit the partial derivatives of the deformation with respect to the spatial coordinates, because these derivatives cannot be evaluated on points of discontinuity in the deformation. Peridynamic equations are integro-differential equations rather than partial differential equations. The resulting theory is *strongly nonlocal* in that it allows direct interaction, through a material model, of material points that are separated by a finite distance. Introductions to peridynamic theory can be found in Silling (2000); Silling and Lehoucq (2010) and Madenci and Oterkus (2014).

p0045 One way of deriving peridynamic equations is to consider the strain energy density $W(\mathbf{x})$ at a point $\mathbf{x}$ in a body $\mathcal{B}$. In the peridynamic model, the strain energy density is determined by the deformation of all the material in a neighborhood $\mathcal{H}_{\mathbf{x}}$ centered at $\mathbf{x}$ with radius $\delta > 0$. The maximum interaction distance δ is called the *horizon* of the material and is treated like a material property. The neighborhood $\mathcal{H}_{\mathbf{x}}$ is called the *family* of $\mathbf{x}$ (Figure 12.1). The key distinction between this model and the standard theory is that, in peridynamics, $W(\mathbf{x})$ is determined by the collective deformation of all the points in $\mathcal{H}_{\mathbf{x}}$, rather than the deformation gradient at $\mathbf{x}$.

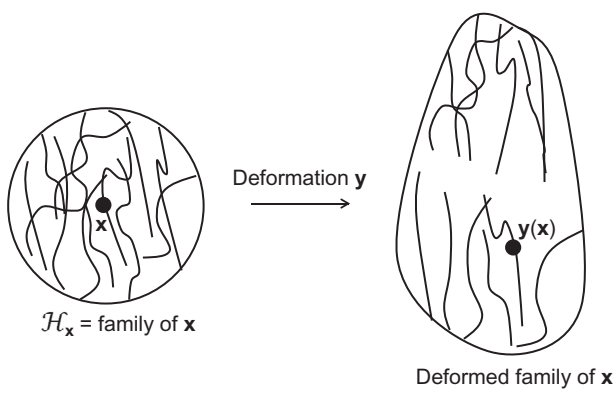

f0010 **Figure 12.1** The strain energy density at a material point $\mathbf{x}$ is determined by the deformation of its family.

Comp. by: KKalaiselvi Stage: Proof Chapter No.: 12 Title Name: Camanho
Date:23/4/15 Time:13:18:57 Page Number: 333

To protect the rights of the author(s) and publisher we inform you that this PDF is an uncorrected proof for internal business use only by the author(s), editor(s), reviewer(s), Elsevier and typesetter SPi. It is not allowed to publish this proof online or in print. This proof copy is the copyright property of the publisher and is confidential until formal publication.

B978-0-08-100332-9.00012-8, 00012

p0050 To represent the dependence of W on the deformation of $\mathcal{H}_{\mathbf{x}}$ requires the use of mathematical objects called *states*, which are simply mappings defined on $\mathcal{H}_{\mathbf{x}}$. The deformation within $\mathcal{H}_{\mathbf{x}}$ is represented by the *deformation state* $\underline{\mathbf{Y}}[\mathbf{x}]$ defined by

$$\underline{\mathbf{Y}}[\mathbf{x}]\langle \mathbf{q}-\mathbf{x}\rangle = \mathbf{y}(\mathbf{q}) - \mathbf{y}(\mathbf{x}), \tag{12.1}$$

where $\mathbf{q} \in \mathcal{H}_{\mathbf{x}}$. The relative position vector $\mathbf{q}-\mathbf{x}$ is called the *bond* from $\mathbf{x}$ to $\mathbf{q}$, which is henceforth noted as $\boldsymbol{\xi}$. Thus, the deformation state maps any bond onto its image under deformation $\mathbf{y}$ (Figure 12.2). In an elastic peridynamic material, the dependence Au1 of the strain energy density on the deformation of the family is represented by

$$W(\mathbf{x}) = \hat{W}(\underline{\mathbf{Y}}[\mathbf{x}]), \tag{12.2}$$

where $\hat{W}$ is the material model. The key idea is that W depends on the *mapping* of $\mathcal{H}_{\mathbf{x}}$ onto its deformed image, not just on the deformation of particular bonds.

p0055 The potential energy Φ corresponding to a deformation field $\mathbf{y}$ in a bounded elastic body subjected to external body force density field $\mathbf{b}$ is given by

$$\Phi = \int_{\mathcal{B}} (W(\mathbf{x}) - \mathbf{b}(\mathbf{x}) \cdot \mathbf{y}(\mathbf{x}))\, \mathrm{d}V_{\mathbf{x}}, \tag{12.3}$$

which is formally the same as in the standard theory. To obtain the equilibrium equation, the first variation of Φ is evaluated with respect to $\mathbf{y}$. The Euler–Lagrange equation corresponding to stationary Φ is then found to be

$$\int_{\mathcal{H}_{\mathbf{x}}} (\mathbf{t}(\mathbf{q},\mathbf{x}) - \mathbf{t}(\mathbf{x},\mathbf{q}))\, \mathrm{d}V_{\mathbf{q}} + \mathbf{b}(\mathbf{x}) = \mathbf{0} \tag{12.4}$$

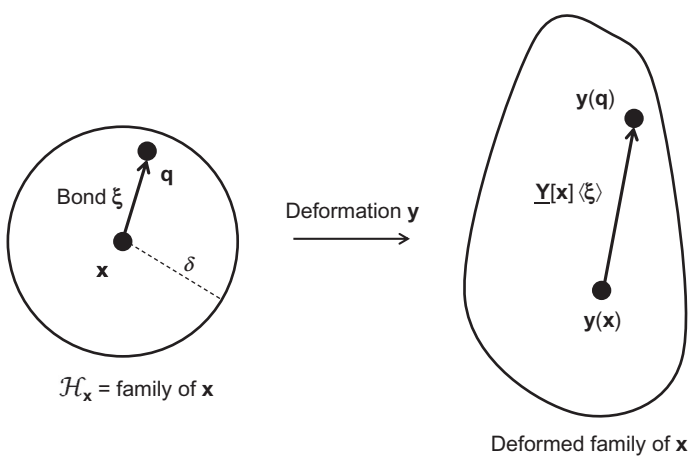

f0015 **Figure 12.2** Point $\mathbf{x}$ is connected to its neighbors $\mathbf{q}$ by bonds. The deformation state maps these bonds into their images under deformation.

Comp. by: KKalaiselvi Stage: Proof Chapter No.: 12 Title Name: Camanho
Date:23/4/15 Time:13:18:58 Page Number: 334

To protect the rights of the author(s) and publisher we inform you that this PDF is an uncorrected proof for internal business use only by the author(s), editor(s), reviewer(s), Elsevier and typesetter SPi. It is not allowed to publish this proof online or in print. This proof copy is the copyright property of the publisher and is confidential until formal publication.

B978-0-08-100332-9.00012-8, 00012

for all $\mathbf{x} \in \mathcal{B}$, where $\mathbf{t}(\mathbf{q},\mathbf{x})$ and $\mathbf{t}(\mathbf{x},\mathbf{q})$ are vectors called *bond force densities*. These have dimensions of force/volume^2. They are derived from the material model for strain energy density by

$$\mathbf{t}(\mathbf{q},\mathbf{x}) = \hat{W}_{\underline{\mathbf{Y}}}(\underline{\mathbf{Y}}[\mathbf{x}])\langle \mathbf{q}-\mathbf{x}\rangle, \quad \mathbf{t}(\mathbf{x},\mathbf{q}) = \hat{W}_{\underline{\mathbf{Y}}}(\underline{\mathbf{Y}}[\mathbf{q}])\langle \mathbf{x}-\mathbf{q}\rangle, \tag{12.5}$$

where the symbol $W_{\underline{\mathbf{Y}}}$ denotes the Fréchet derivative of the strain energy density W with respect to the deformation state. The Fréchet derivative has the property that for a small change in the deformation state $d\underline{\mathbf{Y}}$, the corresponding change in the strain energy density at $\mathbf{x}$ is given by

$$\hat{W}(\underline{\mathbf{Y}} + d\underline{\mathbf{Y}}) - \hat{W}(\underline{\mathbf{Y}}) = \hat{W}_{\underline{\mathbf{Y}}} \bullet d\underline{\mathbf{Y}} \tag{12.6}$$

plus higher-order terms, where the inner product of two states is defined by

$$\underline{\mathbf{A}} \bullet \underline{\mathbf{B}} = \int_{\mathcal{H}} \underline{\mathbf{A}}\langle \boldsymbol{\xi}\rangle \cdot \underline{\mathbf{B}}\langle \boldsymbol{\xi}\rangle \, \mathrm{d}V_{\boldsymbol{\xi}}. \tag{12.7}$$

p0060 Thus, $\hat{W}_{\underline{\mathbf{Y}}}$ is the work conjugate of $\underline{\mathbf{Y}}$. For elastic and inelastic materials, the bond force vectors can be regarded as belonging to the *force state* $\underline{\mathbf{T}}$ evaluated for particular bonds, and we write

$$\mathbf{t}(\mathbf{q},\mathbf{x}) = \underline{\mathbf{T}}[\mathbf{x}]\langle \mathbf{q}-\mathbf{x}\rangle, \quad \mathbf{t}(\mathbf{x},\mathbf{q}) = \underline{\mathbf{T}}[\mathbf{q}]\langle \mathbf{x}-\mathbf{q}\rangle. \tag{12.8}$$

p0065 The material model gives the force state as a function of the deformation state and possibly other variables such as temperature θ and rate of change of the deformation state $\underline{\dot{\mathbf{Y}}}$:

$$\underline{\mathbf{T}} = \hat{\underline{\mathbf{T}}}(\underline{\mathbf{Y}}, \underline{\dot{\mathbf{Y}}}, \theta, \ldots). \tag{12.9}$$

p0070 For the special case of an elastic material, we write

$$\hat{\underline{\mathbf{T}}} = \hat{W}_{\underline{\mathbf{Y}}}. \tag{12.10}$$

p0075 An example of a peridynamic material model is given by

$$\hat{W}(\underline{\mathbf{Y}}) = \frac{kv^2}{2}, \; v = \frac{3\int_{\mathcal{H}} \underline{e}\langle \boldsymbol{\xi}\rangle \, \mathrm{d}V_{\boldsymbol{\xi}}}{\int_{\mathcal{H}} |\boldsymbol{\xi}| \, \mathrm{d}V_{\boldsymbol{\xi}}}, \quad \underline{e}\langle \boldsymbol{\xi}\rangle = |\underline{\mathbf{Y}}\langle \boldsymbol{\xi}\rangle| - |\boldsymbol{\xi}|, \tag{12.11}$$

where k is the bulk modulus, v is the nonlocal dilatation, and $\underline{e}$ is the *bond extension state*. The factor of three appears so that this expression for v gives the same value as the conventional dilatation $u_{i,i}$ for deformations that are small and isotropic. For any bond $\boldsymbol{\xi}$, the value of $\underline{e}\langle \boldsymbol{\xi}\rangle$ is the change in length of the bond due to deformation.

Comp. by: KKalaiselvi Stage: Proof Chapter No.: 12 Title Name: Camanho
Date:23/4/15 Time:13:18:58 Page Number: 335

To protect the rights of the author(s) and publisher we inform you that this PDF is an uncorrected proof for internal business use only by the author(s), editor(s), reviewer(s), Elsevier and typesetter SPi. It is not allowed to publish this proof online or in print. This proof copy is the copyright property of the publisher and is confidential until formal publication.

B978-0-08-100332-9.00012-8, 00012

The nonlocal dilatation v is computed from the mean length change in the family as it deforms. The corresponding force state is found from the Fréchet derivative of $\hat{W}$ to be

$$\underline{\hat{\mathbf{T}}}\langle\boldsymbol{\xi}\rangle = \left(\frac{3kv}{\int_{\mathcal{H}}|\boldsymbol{\zeta}|\,\mathrm{d}V_{\boldsymbol{\zeta}}}\right)\underline{\mathbf{M}}\langle\boldsymbol{\xi}\rangle,\quad \underline{\mathbf{M}}\langle\boldsymbol{\xi}\rangle = \frac{\underline{\mathbf{Y}}\langle\boldsymbol{\xi}\rangle}{|\underline{\mathbf{Y}}\langle\boldsymbol{\xi}\rangle|} \tag{12.12}$$

for any bond $\boldsymbol{\xi}\in\mathcal{H}$. In this expression, $\boldsymbol{\zeta}$ is used as the dummy bond variable in the volume integral. The state $\underline{\mathbf{M}}$ contains the deformed bond directions. For this material model, which represents a linear elastic fluid, the bond forces are parallel to the deformed bond vectors. Material models with this property are called *ordinary* material models; all others are called *nonordinary*. Further discussion of this peridynamic fluid material model may be found in Silling et al. (2007).

p0080 A special case of ordinary material models is called *bond-based* materials. These have the property that the force in each bond is determined *only* by the deformation of that particular bond, independently of what happens to the other bonds in the family. An example of a bond-based material model is given by

$$\underline{\hat{\mathbf{T}}}\langle\boldsymbol{\xi}\rangle = C(\boldsymbol{\xi})\underline{e}\langle\boldsymbol{\xi}\rangle\underline{\mathbf{M}}\langle\boldsymbol{\xi}\rangle \tag{12.13}$$

for all $\boldsymbol{\xi}\in\mathcal{H}$. In this material, each bond acts like a linear elastic spring whose spring constant is the scalar-valued micromodulus function C. In *isotropic* bond-based material models (in which $C(\boldsymbol{\xi})$ is independent of the direction of $\boldsymbol{\xi}$), only one elastic modulus can be reproduced and, in three dimensions, the Poisson ratio is always 1/4. This restriction is not true for the more general *state-based* material models, such as the fluid material model discussed above, in which the Poisson ratio is 1/2. The key distinction is that in the fluid model (12.12), the bond forces depend on the collective deformation, embodied in v, of the entire family, whereas in Equation (12.13), each bond's force density depends only on its own deformation. We will see in the next section that a suitable choice of $C(\boldsymbol{\xi})$, especially through its dependence on bond direction, results in a simple way to include anisotropy in a material model.

p0085 A useful example of a nonordinary material model is found in *correspondence* materials. In these materials, a stress–strain relation from the standard theory is adapted to the peridynamic setting. Suppose that we are given such a stress–strain relation in the form

$$\boldsymbol{\sigma}(\mathbf{x}) = \hat{\boldsymbol{\sigma}}(\mathbf{F}(\mathbf{x})),\quad \mathbf{F}(\mathbf{x}) = \frac{\partial\mathbf{y}}{\partial\mathbf{x}}(\mathbf{x})$$

for any $\mathbf{x}\in\mathcal{B}$, where $\boldsymbol{\sigma}$ is the Piola stress. In the correspondence approach, a *nonlocal deformation gradient* $\bar{\mathbf{F}}(\underline{\mathbf{Y}})$ is computed from

$$\bar{\mathbf{F}} = \left(\int_{\mathcal{H}}\omega(|\boldsymbol{\xi}|)\underline{\mathbf{Y}}\langle\boldsymbol{\xi}\rangle\otimes\boldsymbol{\xi}\,\mathrm{d}V_{\boldsymbol{\xi}}\right)\mathbf{K}^{-1},\quad \mathbf{K} = \int_{\mathcal{H}}\omega(|\boldsymbol{\xi}|)\boldsymbol{\xi}\otimes\boldsymbol{\xi}\,\mathrm{d}V_{\boldsymbol{\xi}}, \tag{12.14}$$

Comp. by: KKalaiselvi Stage: Proof Chapter No.: 12 Title Name: Camanho
Date:23/4/15 Time:13:18:58 Page Number: 336

To protect the rights of the author(s) and publisher we inform you that this PDF is an uncorrected proof for internal business use only by the author(s), editor(s), reviewer(s), Elsevier and typesetter SPi. It is not allowed to publish this proof online or in print. This proof copy is the copyright property of the publisher and is confidential until formal publication.

B978-0-08-100332-9.00012-8, 00012

where ω is a weighting function called the *influence function*. As discussed in Silling et al. (2007), this nonlocal deformation gradient agrees with the conventional deformation gradient $\mathbf{F} = \partial\,\mathbf{y}/\partial\,\mathbf{x}$ whenever the deformation is uniform; that is, whenever $\mathbf{F}$ is constant. The force state is then found from

$$\underline{\hat{\mathbf{T}}}\,\langle\boldsymbol{\xi}\rangle = \omega(|\boldsymbol{\xi}|)\hat{\boldsymbol{\sigma}}(\bar{\mathbf{F}})\mathbf{K}^{-1}\boldsymbol{\xi} \tag{12.15}$$

for any bond $\boldsymbol{\xi} \in \mathcal{H}$. If $\hat{\boldsymbol{\sigma}}$ is elastic, then the peridynamic correspondence material model is also elastic, and the strain energy density function $\hat{W}$ agrees with the one in the standard model whenever the deformation is uniform.

p0090 Correspondence models are useful because they allow material models in the standard theory to be "recycled" without deriving a peridynamic model from scratch. However, they suffer from some practical limitations owing to the fact that in general they are noninvertible. That is, for a given $\underline{\mathbf{T}}$, there are usually an infinite number of choices of $\underline{\mathbf{Y}}$ such that $\underline{\mathbf{T}} = \underline{\hat{\mathbf{T}}}(\underline{\mathbf{Y}})$ if a correspondence model is used. This noninvertibility has implications for material stability and, unless corrective terms are introduced, results in troublesome zero-energy modes in particle type numerical discretizations. These undesirable behaviors, along with innovative approaches to controlling them, are discussed in Littlewood (2010), Tupek et al. (2013), Tupek and Radovitzky (2014), and Breitenfeld et al. (2014).

p0095 Damage is modeled by including a dependence on the *damage state* $\underline{\phi}$ in the material model:

$$\underline{\mathbf{T}} = \underline{\hat{\mathbf{T}}}(\underline{\mathbf{Y}}, \underline{\phi}). \tag{12.16}$$

p0100 The damage state is a scalar-valued state that, for each bond, varies from 0 (undamaged) to 1 (fully damaged). For each bond $\boldsymbol{\xi}$, $\underline{\phi}\langle\boldsymbol{\xi}\rangle$ is a nondecreasing function of time. Commonly, damage in a bond is treated as *bond breakage* in which $\underline{\phi}\langle\boldsymbol{\xi}\rangle$ jumps discontinuously from 0 to 1 according to some criterion. A breakage criterion that is often used in numerical simulations is *critical bond strain*. In this approach, each bond is assigned a critical value $s_*\langle\boldsymbol{\xi}\rangle$. The damage in the bond jumps irreversibly from 0 to 1 when the bond strain $s\langle\boldsymbol{\xi}\rangle$ exceeds $s_*\langle\boldsymbol{\xi}\rangle$, where the bond strain is defined by

$$s\langle\boldsymbol{\xi}\rangle = \frac{e\langle\boldsymbol{\xi}\rangle}{|\boldsymbol{\xi}|} \tag{12.17}$$

for any bond $\boldsymbol{\xi} \in \mathcal{H}$. In practice, if a peridynamic continuum is viewed as a complex network of bonds going in every direction, the breakage of an individual bond makes it more likely that its neighbors will also break, because more load is shifted to these neighbors. As more and more bonds break, a progressive process of failure occurs in the continuum. This process may be either stable or unstable, depending on the geometry and loading conditions. In three dimensions, the geometry of the failed regions usually organizes into two-dimensional surfaces, possibly curved, that we interpret as cracks. Thanks to the compatibility of the peridynamic field equations with discontinuities, cracks form spontaneously and without restriction or

Comp. by: KKalaiselvi Stage: Proof Chapter No.: 12 Title Name: Camanho
Date:23/4/15 Time:13:18:58 Page Number: 337

To protect the rights of the author(s) and publisher we inform you that this PDF is an uncorrected proof for internal business use only by the author(s), editor(s), reviewer(s), Elsevier and typesetter SPi. It is not allowed to publish this proof online or in print. This proof copy is the copyright property of the publisher and is confidential until formal publication.

B978-0-08-100332-9.00012-8, 00012

supplemental kinetic relations that are needed in traditional fracture mechanics. In particular, the concept of a stress intensity factor is not needed in peridynamics.

p0105 In a model of a brittle elastic solid, the critical bond strain can be calibrated to match the critical energy release rate of the material (Silling and Askari, 2005). We will see in the next section that allowing dependence of $s_*\langle\boldsymbol{\xi}\rangle$ on the direction of $\boldsymbol{\xi}$ provides a simple way to model anisotropy in material fracture and failure.

p0110 Peridynamic equations can be linearized under the assumption of small displacement (not necessarily the small displacement gradient). The resulting equilibrium equation has the following form:

$$\int_{\mathcal{N}_{\mathbf{x}}} \mathbf{C}(\mathbf{x},\mathbf{q})(\mathbf{u}(\mathbf{q})-\mathbf{u}(\mathbf{x}))\,\mathrm{d}V_{\mathbf{q}}+\mathbf{b}(\mathbf{x})=\mathbf{0}, \tag{12.18}$$

where $\mathbf{C}$ is the tensor-valued micromodulus field, $\mathbf{u}(\mathbf{x})=\mathbf{y}(\mathbf{x})-\mathbf{x}$ is the displacement field, and $\mathcal{N}_{\mathbf{x}}$ is a neighborhood of $\mathbf{x}$. In general, the radius of $\mathcal{N}_{\mathbf{x}}$ is 2δ, where δ is the horizon of the underlying nonlinear material model that is being linearized (Silling, 2010). The linearized equilibrium equation is formally the same as in Kunin's nonlocal theory (Kunin, 1983).

s0020 12.3 Peridynamic material models for composites

p0115 Here we discuss some methods for treating unidirectional reinforced laminates with peridynamics. Most published peridynamic models for composites are homogenized; that is, they involve smoothed material property fields that do not explicitly include heterogeneities. Because of its nonlocal nature, peridynamics offers opportunities for studying aspects of composite mechanics that are not easily reproduced in standard local theory. Due to their heterogeneous composition, nonlocal interactions appear whenever composites are represented with smoothed displacement fields. This nonlocality occurs not because of physical interactions across finite distances, as in electrostatics, but because of the tendency of the material phases to readjust individually relative to each other when only their averaged value is specified. The resulting exchange of forces between the phases occurs over finite distances that can be estimated using, for example, a shear lag type of analysis. The length scale for these interactions involves not only geometrical length scales (fiber diameter, ply thickness, etc.) but also the relative material properties of the phases (Silling, 2014).

p0120 One way of modeling a unidirectionally reinforced lamina with peridynamics is to use the correspondence approach discussed in the previous section. Any stress–strain model for a lamina from standard lamination theory can be directly incorporated into a peridynamic model using correspondence. The resulting peridynamic model has the same characteristics as the standard model for reproducing the anisotropic elastic properties of a lamina. All four independent elastic moduli can be reproduced (Jones, 1999). The correspondence approach can also be applied to a three-dimensional model of a laminate, introducing a fifth elastic modulus that can be

Comp. by: KKalaiselvi Stage: Proof Chapter No.: 12 Title Name: Camanho
Date:23/4/15 Time:13:18:58 Page Number: 338

To protect the rights of the author(s) and publisher we inform you that this PDF is an uncorrected proof for internal business use only by the author(s), editor(s), reviewer(s), Elsevier and typesetter SPi. It is not allowed to publish this proof online or in print. This proof copy is the copyright property of the publisher and is confidential until formal publication.

B978-0-08-100332-9.00012-8, 00012

specified independently, as in lamination theory. The correct A and D matrices are predicted by the peridynamic correspondence model for any orientation of the plies in an arbitrarily chosen layup.

p0125 Because the correspondence approach borrows a stress–strain relation from the standard theory, it is suitable for the application of failure models, such as the Hashin model, that are based on components of the stress tensor (Hashin, 1980). Such a failure model can be represented as a surface in the stress space of the form

$$\psi(\boldsymbol{\sigma}, a_1, a_2, \ldots, a_N) < \psi_0 \tag{12.19}$$

for a nonfailed material, where $\boldsymbol{\sigma}$ is the stress tensor and $\psi_0, a_1, a_2, \ldots, a_N$ are parameters for the failure model calibrated for a material. In the correspondence model, failure occurs when the condition

$$\psi(\hat{\boldsymbol{\sigma}}(\bar{\mathbf{F}}), a_1, a_2, \ldots, a_N) < \psi_0 \tag{12.20}$$

fails to hold, where $\bar{\mathbf{F}}$ is the nonlocal deformation gradient tensor discussed previously.

p0130 When failure occurs according this condition, the next question is how to translate this event into bond damage. Many ways are possible. One approach is to break the "worst" bond, that is, the bond that should break first on the basis of physical intuition or because of some condition derived from the failure model. For example, the peridynamic bond damage model could break the bond within the family of a point $\mathbf{x}$ that has the greatest tensile bond strain, assuming that the material is failing under tension. For failure under compression, the model could break the bond with the greatest compressive strain. The difficulty here is that in the Hashin model, there are an infinite number of combinations of stress components that result in failure. These infinite combinations therefore introduce an ad hoc character to the peridynamic model in trying to identify the "worst" bond by introducing an extraneous bond failure criterion.

p0135 An alternative is to use the failure surface ψ more directly to identify bond damage. One way to do this is to evaluate the gradient of this surface, in the sense of Fréchet derivatives, with respect to the deformation state. Using the chain rule leads to

$$\psi_{\underline{\mathbf{Y}}} = \frac{\partial \psi}{\partial \boldsymbol{\sigma}} \cdot \frac{\partial \hat{\boldsymbol{\sigma}}}{\partial \mathbf{F}} \cdot \bar{\mathbf{F}}_{\underline{\mathbf{Y}}}. \tag{12.21}$$

p0140 Here, the Fréchet derivative $\bar{\mathbf{F}}_{\underline{\mathbf{Y}}}$ is computed from Equations (12.6) and (12.14). The term $\partial\hat{\boldsymbol{\sigma}}/\partial\mathbf{F}$ is the fourth-order elasticity tensor for an incremental deformation. Under the assumption that bond damage occurs preferentially in those bonds that contribute the most to $\psi_{\underline{\mathbf{Y}}}$, a possible bond damage model is then

$$\underline{\dot{\phi}}\,\langle \boldsymbol{\xi} \rangle = \lambda \psi_{\underline{\mathbf{Y}}} \langle \boldsymbol{\xi} \rangle \tag{12.22}$$

for any bond $\boldsymbol{\xi} \in \mathcal{H}$, where $\lambda > 0$ is independent of $\boldsymbol{\xi}$. Continuum damage models can be similarly adapted to peridynamics.

Comp. by: KKalaiselvi Stage: Proof Chapter No.: 12 Title Name: Camanho
Date:23/4/15 Time:13:18:58 Page Number: 339

To protect the rights of the author(s) and publisher we inform you that this PDF is an uncorrected proof for internal business use only by the author(s), editor(s), reviewer(s), Elsevier and typesetter SPi. It is not allowed to publish this proof online or in print. This proof copy is the copyright property of the publisher and is confidential until formal publication.

p0145 Most of the published peridynamic lamina models are bond-based. Among these are the models of Askari et al. (2006), Xu et al. (2007, 2008), Hu et al. (2011, 2012), Hu et al. (2014), and Liu and Jia (2012). In these models, anisotropy is introduced by giving special properties to bonds that are parallel to the fiber direction in the undeformed configuration. These bonds are called *fiber bonds*; all other bonds in the lamina model are called *matrix bonds*. Referring to the bond-based expression (12.13), and using a coordinate system in which x_1 is parallel to the fibers, the scalar micromodulus of a bond in the plane of the lamina may be written as

$$C(\boldsymbol{\xi}) = C_m(|\boldsymbol{\xi}|) + C_f(|\boldsymbol{\xi}|)\Delta(\xi_2), \tag{12.23}$$

where Δ denotes the Dirac delta function. Applying this material model in the peridynamic equilibrium equation (12.4) results in

$$\int_{\mathcal{H}} C_m(|\boldsymbol{\xi}|)\underline{e}\langle\boldsymbol{\xi}\rangle\underline{\mathbf{M}}\langle\boldsymbol{\xi}\rangle\,\mathrm{d}V_{\boldsymbol{\xi}} + \int_{\mathcal{L}} C_f(|\boldsymbol{\xi}|)\underline{e}\langle\boldsymbol{\xi}\rangle\underline{\mathbf{M}}\langle\boldsymbol{\xi}\rangle\,\mathrm{d}\ell_{\boldsymbol{\xi}} + \mathbf{b}(\mathbf{x}) = \mathbf{0}, \tag{12.24}$$

where $\mathcal{L}$ is the line segment $[-\delta,\delta]$ along the x_1-axis and $\ell_{\boldsymbol{\xi}}$ is the path length in the line integral. The second integral sums up the forces in the fiber bonds. In this form, it is easy to see the strength of the peridynamic formulation for composites: the fiber bonds need not deform continuously with the matrix bonds, allowing the exploration of deformations in which the fibers separate from the matrix.

p0150 Bond-based material models for composites are compatible with simple bond breakage models that allow interesting damage progression phenomena to be reproduced. Using a critical bond strain breakage criterion, we can allow fiber bonds to have a critical strain that is independent of the matrix bond critical strain. Laminas can be anisotropic in damage formation as well as in elastic response. Compressive failure in a lamina can be modeled using a critical bond strain criterion under compression as well as under tension.

p0155 Bond-based lamina models can be assembled into laminate models with arbitrary stacking sequences. Additional bonds, with their own elastic and failure properties, connect points within the laminas. These *interlayer* bonds can extend only between neighboring plies or over multiple plies, according to the modeling assumptions one wishes to make. A critical bond strain failure criterion for interlayer bonds can be calibrated to match the tensile and shear energy release rates, G_{Ic} or G_{IIc}, for delaminations, but not both of these constants independently. More flexibility can be obtained with alternative failure criteria for interlayer bonds. For example, interlayer bonds can be considered to fail when the shear angle between neighboring plies exceeds some critical angle (Oterkus, 2010; Oterkus et al., 2012). When applied together with a critical tensile bond strain criterion, measured energy release rates in both tensile and shear modes can be reproduced during delamination. Bond-based models for composites, coupled with conventional finite element models, have been successfully applied to the failure of large aerospace structures (Oterkus et al., 2012). Later sections in this chapter discuss the coupling of peridynamics with finite element

Comp. by: KKalaiselvi Stage: Proof Chapter No.: 12 Title Name: Camanho
Date:23/4/15 Time:13:18:59 Page Number: 340

To protect the rights of the author(s) and publisher we inform you that this PDF is an uncorrected proof for internal business use only by the author(s), editor(s), reviewer(s), Elsevier and typesetter SPi. It is not allowed to publish this proof online or in print. This proof copy is the copyright property of the publisher and is confidential until formal publication.

B978-0-08-100332-9.00012-8, 00012

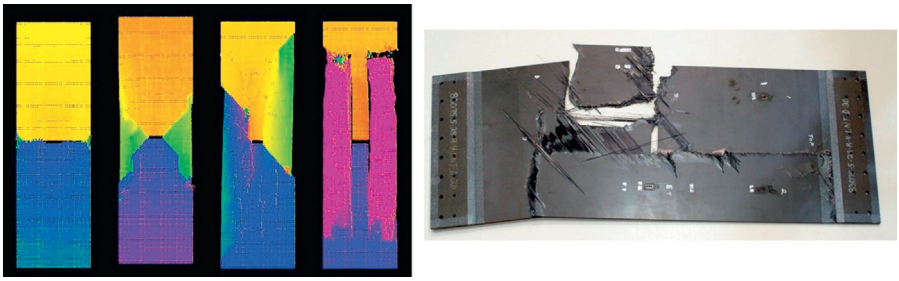

f0020 **Figure 12.3** Left: Simulated damage patterns using a bond-based peridynamic model. Right: The result of a typical test.

meshes. A bond-based mechanical model has also been coupled with a peridynamic heat conduction model for composites (Oterkus and Madenci, 2014).

p0160 Bond-based laminate models with anisotropic critical bond strain breakage criteria can reproduce a surprisingly large spectrum of damage phenomena in composites. An example is shown in Figure 12.3, which shows the failure of laminates in simulated large-notch tension (LNT) tests, along with a typical experimental result. Figure 12.4 shows delaminations predicted due to impact from a rigid projectile using the shear bond approach. It also shows computed compressive failure in a model of compression after impact (CAI).

p0165 Unlike the correspondence models, bond-based material models for composites cannot match all four independent elastic moduli in laminas. Because, in effect, C_m and C_f act like independent parameters for purposes of calibrating the elastic properties of the model, only two elastic moduli can be reproduced by manipulating these two parameters. A modification of the bond-based model described above that includes a dependence of C_m on the bond angle as well as the length (that is, $C_m(\boldsymbol{\xi})$ instead of $C_m(|\boldsymbol{\xi}|)$) allows three elastic moduli to be matched.

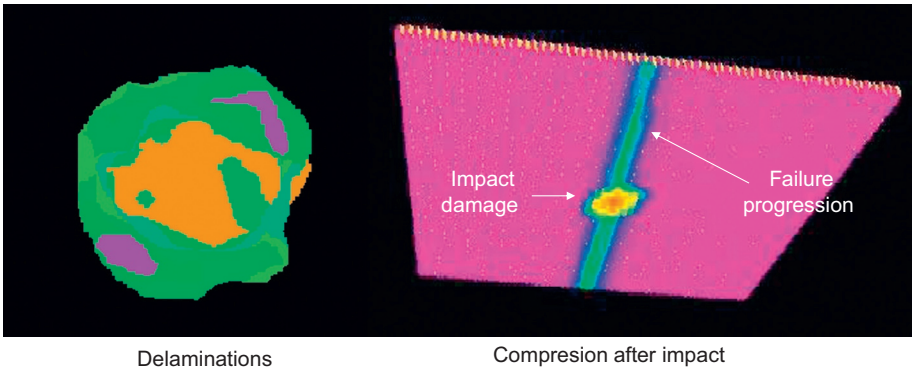

f0025 **Figure 12.4** Left: Simulated delaminations caused by impact (viewed from impacted side). Right: Compression after impact.

Comp. by: KKalaiselvi Stage: Proof Chapter No.: 12 Title Name: Camanho
Date:23/4/15 Time:13:18:59 Page Number: 341

To protect the rights of the author(s) and publisher we inform you that this PDF is an uncorrected proof for internal business use only by the author(s), editor(s), reviewer(s), Elsevier and typesetter SPi. It is not allowed to publish this proof online or in print. This proof copy is the copyright property of the publisher and is confidential until formal publication.

B978-0-08-100332-9.00012-8, 00012

p0170 Kilic et al. (2009) introduced a nonhomogenized bond-based lamina representation. In their approach, structures representing fibers are explicitly included in the lamina. These structures are discretized in detail in the numerical model. This approach has the advantage of reproducing some features of composite responses that are the outcome of the heterogeneity of the mesoscale. However, the price paid is the introduction of features that have a much larger size than the actual fibers they represent.

p0175 Another approach to peridynamic modeling of a lamina that allows all four elastic moduli to be matched, yet provides many of the advantages of the bond-based model, is to use an ordinary state-based model (Colavito et al., 2013; Barut et al., 2014). Recall that in ordinary state-based models, the bond force density vector is always parallel to the deformed bond, but the force density can depend on the deformation of other bonds in the family. This allows a volume-dependent term to be included in the lamina model, as well as an angle-dependent matrix bond micromodulus. The resulting expression for bond force then typically takes the form

$$\underline{\hat{\mathbf{T}}}\langle\boldsymbol{\xi}\rangle = \left[\left(C_m(\boldsymbol{\xi}) + C_f(|\boldsymbol{\xi}|)\Delta(\xi_2)\left(\underline{e}\langle\boldsymbol{\xi}\rangle + av\right)\right]\underline{\mathbf{M}}\langle\boldsymbol{\xi}\rangle, \tag{12.25}$$

where a is a constant and v is the two-dimensional dilatation,

$$v = \frac{2\int_{\mathcal{H}} \underline{e}\langle\boldsymbol{\xi}\rangle \, \mathrm{d}V_{\boldsymbol{\xi}}}{\int_{\mathcal{H}} |\boldsymbol{\xi}| \, \mathrm{d}V_{\boldsymbol{\xi}}}. \tag{12.26}$$

Here, $\mathcal{H}$ refers to the family in the plane of the lamina.

s0025 12.4 Toward a novel treatment of localization

p0180 Peridynamic theory has provided promising results for simulating the failure of composites. For any point in a body, however, peridynamic models must account for all interactions exerted by other points in the neighborhood of this point. This results in a huge computational cost. The morphing coupling method is able to constrain the peridynamic model to small but critical domains, such as the damage nucleation or fracture regions, while a conventional contact-force-based continuum mechanics model is employed over the rest of the structure. Based on the work presented in Lubineau et al. (2012) and Azdoud et al. (2013, 2014), the morphing coupling method is stated as follows.

p0185 For simplicity, we focus on a bond-based peridynamic model for linearized elastic materials. The equilibrium equation of the peridynamic model has been shown in Equation (12.4). A possible bond-based constitutive model is given by

$$\mathbf{t}(\mathbf{q},\mathbf{x}) = \frac{C(\mathbf{x},|\boldsymbol{\xi}|)}{2}\{u_{\boldsymbol{\xi}}(\mathbf{q}) - u_{\boldsymbol{\xi}}(\mathbf{x})\}\boldsymbol{\gamma}_{\boldsymbol{\xi}}, \tag{12.27}$$

Comp. by: KKalaiselvi Stage: Proof Chapter No.: 12 Title Name: Camanho
Date:23/4/15 Time:13:19:04 Page Number: 342

To protect the rights of the author(s) and publisher we inform you that this PDF is an uncorrected proof for internal business use only by the author(s), editor(s), reviewer(s), Elsevier and typesetter SPi. It is not allowed to publish this proof online or in print. This proof copy is the copyright property of the publisher and is confidential until formal publication.

B978-0-08-100332-9.00012-8, 00012

where the bond $\boldsymbol{\xi} = \mathbf{q} - \mathbf{x}$ is the relative position vector, $C(\mathbf{x},|\boldsymbol{\xi}|)$ denotes the micromodulus at point $\mathbf{x}$, which is a function of the length of $\boldsymbol{\xi}$, $\boldsymbol{\gamma}_{\xi} = \boldsymbol{\xi}/|\boldsymbol{\xi}|$ is the direction of bond $\boldsymbol{\xi}$ in the reference configuration, and $u_{\xi}(\mathbf{q})$ denotes the projection of the displacement $\mathbf{u}(\mathbf{q})$ at point $\mathbf{q}$ to the bond $\boldsymbol{\xi}$ (i.e., $u_{\xi}(\mathbf{q}) = \mathbf{u}(\mathbf{q}) \cdot \boldsymbol{\gamma}_{\xi}$) (Lubineau et al., 2012).

p0190 We consider a complete domain $\mathcal{B}$. This domain $\mathcal{B}$ consists of three subdomains, $\mathcal{B}_1$, $\mathcal{B}_2$, and $\mathcal{B}_m$, that is, $\mathcal{B} = \mathcal{B}_1 \cup \mathcal{B}_2 \cup \mathcal{B}_m$, $\mathcal{B}_1 \cap \mathcal{B}_2 = \emptyset$, $\mathcal{B}_1 \cap \mathcal{B}_m = \emptyset$, and $\mathcal{B}_2 \cap \mathcal{B}_m = \emptyset$. For definiteness and without major restrictions, we assume that $\mathcal{B}_2$ is totally embedded within $\mathcal{B}_m$ and that $\mathcal{B}_m$ is totally embedded within $\mathcal{B}_1$, such that $\partial\mathcal{B}_2 \cap \partial\mathcal{B}_1 = \emptyset$ and $\partial\mathcal{B} \subset \partial\mathcal{B}_1$. Therefore, $\mathcal{B}_m$ becomes a transition domain between $\mathcal{B}_1$ and $\mathcal{B}_2$ (see Figure 12.5).

p0195 Let the subdomains $\mathcal{B}_1$ and $\mathcal{B}_2$ be treated by the conventional continuum model and the peridynamic model, respectively. We mainly focus on the finite morphing domain, $\mathcal{B}_m$, where both models coexist and work cooperatively. The displacement, $\bar{\mathbf{u}}$, is imposed on the part $\partial\mathcal{B}_{\mathbf{u}}$ of $\partial\mathcal{B}$, and the surface force $\bar{\mathbf{f}}$ is imposed on the complementary part $\partial\mathcal{B}_{\mathbf{f}}$ of $\partial\mathcal{B}$. In addition, the whole domain $\mathcal{B}$ is subjected to body forces denoted by $\mathbf{b}$.

p0200 The morphing technique is then defined as a simple evolution of the material properties characterizing each model. The morphing coupling method is proposed by the following set of equations that represent a hybrid continuum/peridynamic model:

u0010 □ **Kinematic admissibility and compatibility**

$$\boldsymbol{\epsilon}(\mathbf{x}) = \frac{1}{2}\left(\nabla\mathbf{u}(\underline{x}) + (\nabla\mathbf{u})^{\mathrm{T}}(\underline{x})\right) \qquad \forall\mathbf{x} \in \mathcal{B}\backslash\mathcal{B}_2, \tag{12.28}$$

$$\eta_{\xi}(\mathbf{q},\mathbf{x}) = u_{\xi}(\mathbf{q}) - u_{\xi}(\mathbf{x}) \qquad \forall(\mathbf{q},\mathbf{x}) \in \mathcal{B}\backslash\mathcal{B}_1, \tag{12.29}$$

$$\mathbf{u}(\mathbf{x}) = \bar{\mathbf{u}}(\mathbf{x}) \qquad \forall\mathbf{x} \in \partial\mathcal{B}_{\mathbf{u}}. \tag{12.30}$$

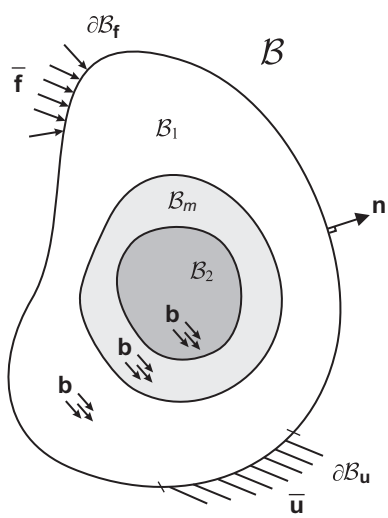

f0030 **Figure 12.5** The whole domain $\mathcal{B}$ consists of $\mathcal{B}_1$, $\mathcal{B}_2$, and $\mathcal{B}_m$.

Comp. by: KKalaiselvi Stage: Proof Chapter No.: 12 Title Name: Camanho
Date:23/4/15 Time:13:19:04 Page Number: 343

To protect the rights of the author(s) and publisher we inform you that this PDF is an uncorrected proof for internal business use only by the author(s), editor(s), reviewer(s), Elsevier and typesetter SPi. It is not allowed to publish this proof online or in print. This proof copy is the copyright property of the publisher and is confidential until formal publication.

u0015 □ **Static admissibility**

$$\div\boldsymbol{\sigma}(\mathbf{x})+\int_{\mathcal{H}_{\mathbf{x}}}\{\mathbf{t}(\mathbf{q},\mathbf{x})-\mathbf{t}(\mathbf{x},\mathbf{q})\}\,\mathrm{d}V_{\mathbf{q}}=-\mathbf{b}(\mathbf{x}) \qquad \forall\mathbf{x}\in\mathcal{B}, \tag{12.31}$$

$$\boldsymbol{\sigma}(\mathbf{x})\cdot\mathbf{n}(\mathbf{x})=\bar{\mathbf{f}}(\mathbf{x}) \qquad \forall\mathbf{x}\in\partial\mathcal{B}_{\mathbf{f}}. \tag{12.32}$$

u0020 □ **Constitutive equations**

$$\boldsymbol{\sigma}(\mathbf{x})=\mathbf{K}(\mathbf{x}):\boldsymbol{\epsilon}(\mathbf{x}) \qquad \forall\mathbf{x}\in\mathcal{B}\backslash\mathcal{B}_2, \tag{12.33}$$

$$\mathbf{t}(\mathbf{q},\mathbf{x})=\frac{C(\mathbf{x},|\boldsymbol{\xi}|)}{2}\eta_{\boldsymbol{\xi}}(\mathbf{q},\mathbf{x})\boldsymbol{\gamma}_{\boldsymbol{\xi}} \qquad \forall\mathbf{x}\in\mathcal{B}\backslash\mathcal{B}_1. \tag{12.34}$$

p0220 In Equation (12.33), $\mathbf{K}(\mathbf{x})$ is the stiffness tensor of the conventional continuum model at the point $\mathbf{x}$. In Equation (12.34), $C(\mathbf{x},|\boldsymbol{\xi}|)$ is the peridynamic micromodulus at point $\mathbf{x}$. $C(\mathbf{x},|\boldsymbol{\xi}|)$ is defined by using a priori morphing function, α, such that

$$C(\mathbf{x},|\boldsymbol{\xi}|)=\alpha(\mathbf{x})c^0(|\boldsymbol{\xi}|). \tag{12.35}$$

p0225 Based on Equation (12.31), we note that the parameters $\alpha(\mathbf{x})$ and $\mathbf{K}(\mathbf{x})$ determine the particular type of this model, that is, the continuum, peridynamic, or hybrid model, at any material point $\mathbf{x}$ in the whole region $\mathcal{B}$:

u0025 • For a point $\mathbf{x}\in\mathcal{B}$, if and only if

$$\mathbf{K}(\mathbf{x})=\mathbf{K}^0 \quad\text{and}\quad \alpha(\mathbf{q})\equiv 0,\quad \forall\mathbf{q}\in\mathcal{H}_{\mathbf{x}}, \tag{12.36}$$

then this point $\mathbf{x}$ strictly belongs to the conventional continuum model. The strain energy density at this point can be written as

$$W(\mathbf{x})=\frac{1}{2}\boldsymbol{\epsilon}(\mathbf{x}):\mathbf{K}^0:\boldsymbol{\epsilon}(\mathbf{x}). \tag{12.37}$$

u0030 • For a point $\mathbf{x}\in\mathcal{B}$, if and only if

$$\mathbf{K}(\mathbf{x})=\mathbf{0} \quad\text{and}\quad \alpha(\mathbf{q})\equiv 1,\quad \forall\mathbf{q}\in\mathcal{H}_{\mathbf{x}}, \tag{12.38}$$

then this point $\mathbf{x}$ strictly belongs to the peridynamic model. The strain energy density at this point can be written as (see Han and Lubineau, 2012)

$$W(\mathbf{x})=\int_{\mathcal{H}_{\mathbf{x}}}c^0(|\boldsymbol{\xi}|)\frac{\eta_{\boldsymbol{\xi}}^2(\mathbf{q},\mathbf{x})}{4}\,\mathrm{d}V_{\mathbf{q}}. \tag{12.39}$$

u0035 • For a point $\mathbf{x}\in\mathcal{B}$, if and only if

$$\mathbf{K}(\mathbf{x})\neq\mathbf{0} \quad\text{and}\quad \exists\mathbf{q}\in\mathcal{H}_{\mathbf{x}},\quad \text{such that}\quad 0<\alpha(\mathbf{q})<1, \tag{12.40}$$

then we can say this point $\mathbf{x}$ belongs to the hybrid model. The strain energy density at this point can be written as (see Lubineau et al., 2012)

$$W(\mathbf{x})=\frac{1}{2}\boldsymbol{\epsilon}(\mathbf{x}):\mathbf{K}(\mathbf{x}):\boldsymbol{\epsilon}(\mathbf{x})+\int_{\mathcal{H}_{\mathbf{x}}}c^0(|\boldsymbol{\xi}|)\frac{\alpha(\mathbf{x})+\alpha(\mathbf{q})}{2}\frac{\eta_{\boldsymbol{\xi}}^2(\mathbf{q},\mathbf{x})}{4}\,\mathrm{d}V_{\mathbf{q}}. \tag{12.41}$$

To protect the rights of the author(s) and publisher we inform you that this PDF is an uncorrected proof for internal business use only by the author(s), editor(s), reviewer(s), Elsevier and typesetter SPi. It is not allowed to publish this proof online or in print. This proof copy is the copyright property of the publisher and is confidential until formal publication.

p0245 If the material in $\mathcal{B}$ is homogeneous and the body $\mathcal{B}$ is under homogeneous deformation, the strain energy density should be independent of the morphing function α. It means that the strain energy density is the same at some point $\mathbf{x}$ whatever the model. Thus, Equation (12.37) is equal to Equation (12.39), that is,

$$\frac{1}{2}\boldsymbol{\epsilon}(\mathbf{x}):\mathbf{K}^0:\boldsymbol{\epsilon}(\mathbf{x})=\int_{\mathcal{H}_\mathbf{x}} c^0(|\boldsymbol{\xi}|)\frac{\eta_{\boldsymbol{\xi}}^2(\mathbf{q},\mathbf{x})}{4}\,\mathrm{d}V_\mathbf{q}. \tag{12.42}$$

p0250 Let us consider an infinitesimal homogeneous transformation over the small neighborhood of point $\mathbf{x}$ such that

$$\boldsymbol{\epsilon}(\mathbf{q})\simeq\boldsymbol{\epsilon}(\mathbf{x})=\overline{\boldsymbol{\epsilon}}\ \text{ and }\ \eta_{\boldsymbol{\xi}}(\mathbf{q},\mathbf{x})=\frac{\boldsymbol{\xi}\cdot\overline{\boldsymbol{\epsilon}}\cdot\boldsymbol{\xi}}{|\boldsymbol{\xi}|}\quad\forall\mathbf{q}\in\mathcal{H}_\mathbf{x}. \tag{12.43}$$

p0255 Based on Equation (12.43), Equation (12.42) yields

$$\mathbf{K}^0=\int_{\mathcal{H}_\mathbf{x}} c^0(|\boldsymbol{\xi}|)\frac{\boldsymbol{\xi}\otimes\boldsymbol{\xi}\otimes\boldsymbol{\xi}\otimes\boldsymbol{\xi}}{2|\boldsymbol{\xi}|^2}\,\mathrm{d}V_\mathbf{q}. \tag{12.44}$$

Similarly, an equivalence exists between Equations (12.37) and (12.41), and considering Equations (12.43) and (12.44), we have

$$\mathbf{K}(\mathbf{x})=(1-\alpha(\mathbf{x}))\mathbf{K}^0+\int_{\mathcal{H}_\mathbf{x}} c^0(|\boldsymbol{\xi}|)\frac{\alpha(\mathbf{x})-\alpha(\mathbf{q})}{2}\frac{\boldsymbol{\xi}\otimes\boldsymbol{\xi}\otimes\boldsymbol{\xi}\otimes\boldsymbol{\xi}}{2|\boldsymbol{\xi}|^2}\,\mathrm{d}V_\mathbf{q}. \tag{12.45}$$

p0260 The advantage of this method is that we do the coupling only at the level of the constitutive equation. This makes it easy to define the morphing coupling and to conduct it from an algorithmic point of view. That is, for a given function α over region $\mathcal{B}$, the governing equations (12.28)–(12.34) can be directly solved based on the constitutive relations (12.44) and (12.45).

p0265 The coupling qualities have been described by using a one-dimensional example in Lubineau et al. (2012). Some two- or three-dimensional numerical examples in Lubineau et al. (2012) and Azdoud et al. (2013) illustrate the accuracy of the morphing coupling method. Figure 12.6 presents a fracture simulation (Azdoud et al., 2014) that uses an adaptive morphing coupling method. The morphing function α automatically updates itself following the crack propagation, which directly determines the scopes of the peridynamic and continuum models. A simple fracture criterion based on the critical stretch of the bond is used, which was addressed in Section 12.2 of this chapter. Above this critical strain, the bond is broken in an irreversible manner. In the numerical implementation, appropriate discretization schemes, such as the finite element method (FEM) and the discontinuous Galerkin finite element method (DGFEM), are employed with the conventional continuum model and the peridynamic model, respectively. Compared with the application of DGFEM to conventional continuum mechanics (Arnold et al., 2002), it is easier to apply DGFEM to peridynamics without the flux constraint over the boundary of the elements (Chen and Gunzburger, 2011).

Comp. by: KKalaiselvi Stage: Proof Chapter No.: 12 Title Name: Camanho
Date:23/4/15 Time:13:19:04 Page Number: 345

To protect the rights of the author(s) and publisher we inform you that this PDF is an uncorrected proof for internal business use only by the author(s), editor(s), reviewer(s), Elsevier and typesetter SPi. It is not allowed to publish this proof online or in print. This proof copy is the copyright property of the publisher and is confidential until formal publication.

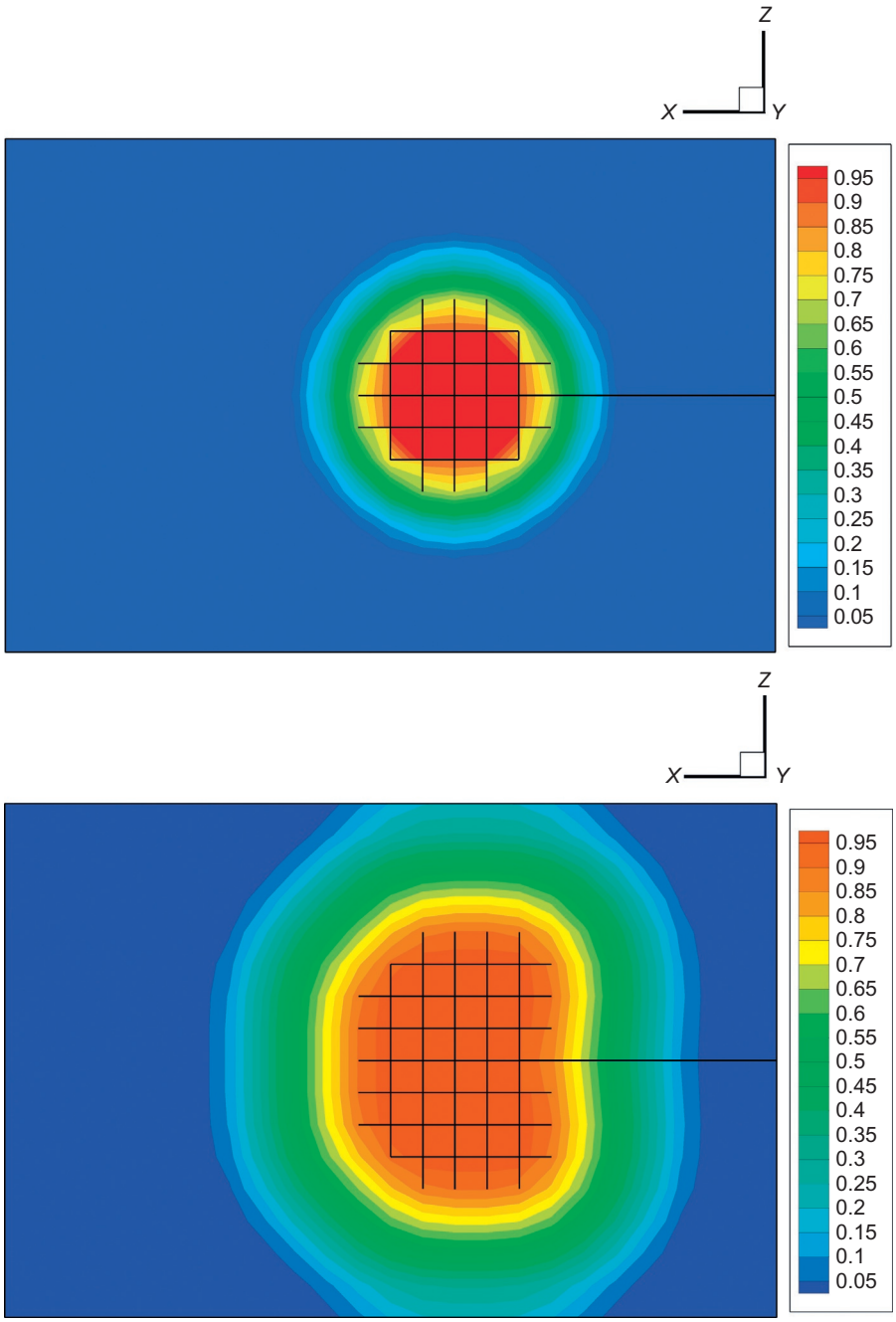

f0035 **Figure 12.6** The evolution of morphing function α on the cross section perpendicular to the y-axis ((a)–(c)) and the dissipated energy in a deformed body ((d)–(f)) under displacement increments (1 increment in (a) and (d), 30 increments in (b) and (e), 50 increments in (c) and (f)). We note that the evolution of the morphing function follows the propagation of the crack. DGFEM, represented by the square element in (a)–(c), is embedded in the peridynamic zone (red) of the cross sections.

(Conitnued)

To protect the rights of the author(s) and publisher we inform you that this PDF is an uncorrected proof for internal business use only by the author(s), editor(s), reviewer(s), Elsevier and typesetter SPi. It is not allowed to publish this proof online or in print. This proof copy is the copyright property of the publisher and is confidential until formal publication.

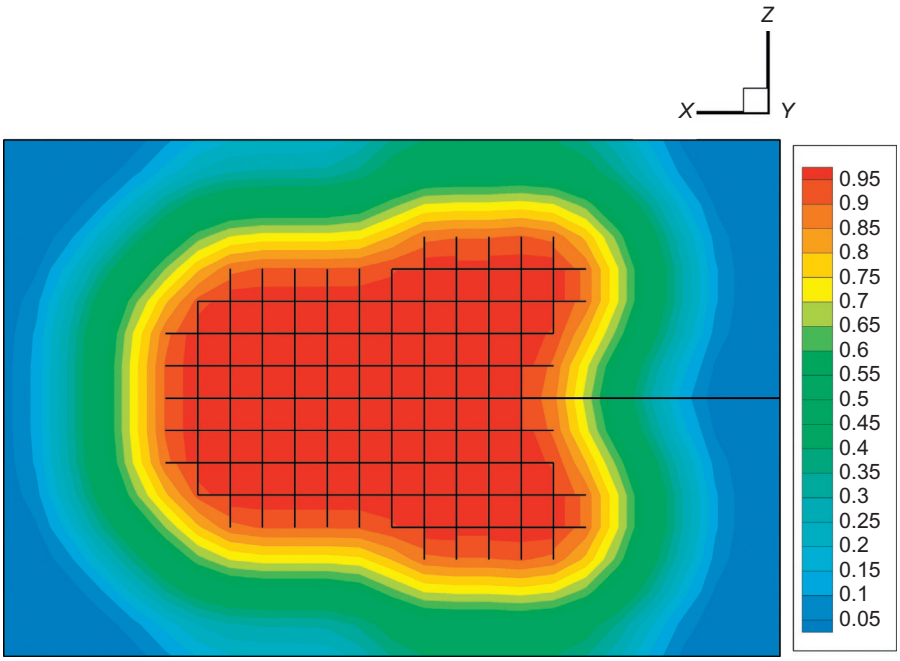

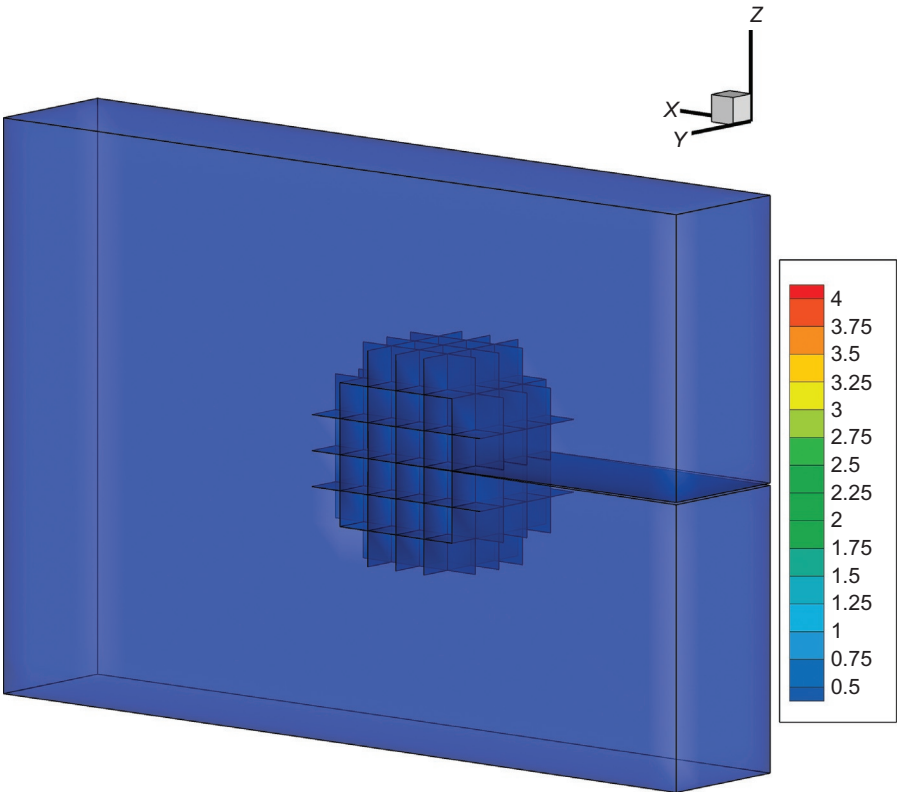

Figure 12.6 Continued

To protect the rights of the author(s) and publisher we inform you that this PDF is an uncorrected proof for internal business use only by the author(s), editor(s), reviewer(s), Elsevier and typesetter SPi. It is not allowed to publish this proof online or in print. This proof copy is the copyright property of the publisher and is confidential until formal publication.

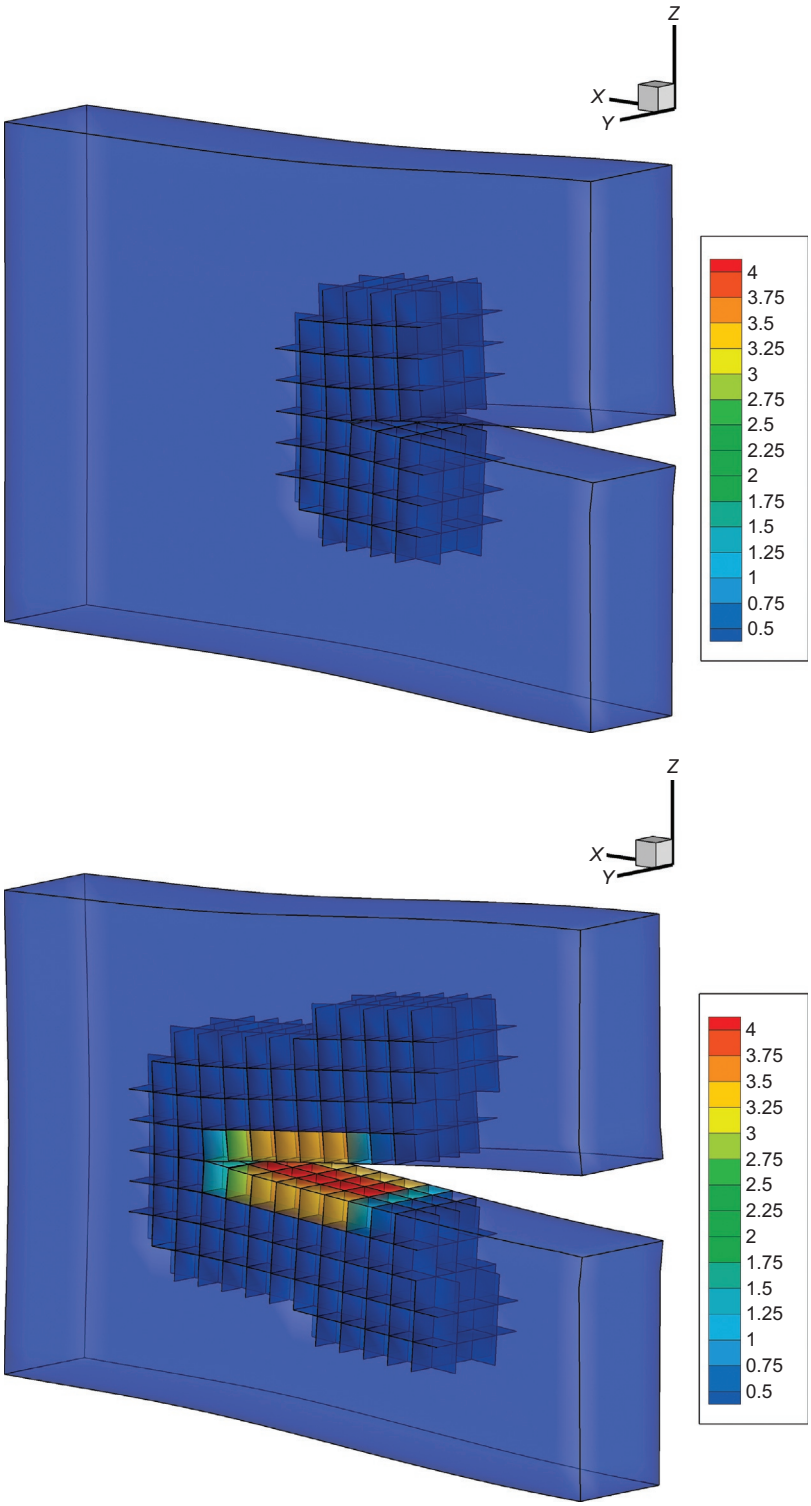

Figure 12.6 Continued

Comp. by: KKalaisel-
No.: 12 Title Name: Ca-

To protect the rights of the author(s) and publisher we inform you that this PDF is an uncorrected proof for internal business use only by the author(s), editor(s), reviewer(s), Elsevier and typesetter SPi. It is not allowed to publish this proof online or in print. This proof copy is the copyright property of the publisher and is confidential until formal publication.

s0030 12.5 Summary

p0270 Peridynamic theory is a recent but powerful and promising solid mechanics framework that can be used for failure analysis of composites materials. Peridynamic models fall into the category of nonlocal mechanics, which allows direct interactions between nonadjacent material points by using integral equations. The connection vector between two points is named a *bond*. Peridynamic damage is modeled by defining a breakage criterion at each bond. The failure process in peridynamics is captured as more and more bonds break in a continuum.

p0275 Here, we considered three peridynamic models for composites: the correspondence model, the bond-based lamina model and the ordinary state-based lamina model. Both the peridynamic correspondence model and the state-based lamina model can reproduce all four independent elastic moduli in lamina, whereas only two elastic moduli can be matched by the bond-based lamina model. Furthermore, a modification of the bond-based model can reproduce three moduli at the most. In addition, the peridynamic correspondence models, which translate stress–strain models from standard lamination theory into bond damage, can be employed for the simulation of failure in composites. The bond-based laminate models with anisotropic bond breakage criteria have been applied to simulate the failure of laminates under LNTs and under CAI. Compared with the bond-based models, the ordinary state-based material model provides more advantages including a volume-dependent term as well as an angle-dependent term.

p0280 An efficient coupling strategy, called the morphing method, is proposed to glue the bond-based peridynamic model to the conventional continuum model. The morphing method couples both models at the level of constitutive parameters in terms of the conservation of strain energy. This capability makes it possible to apply the coupled model to complex structures. And it is possible to extend this strategy to the state-based peridynamic model. Some adaptive fracture simulations have been successfully conducted so far. Future work is required to apply the morphing coupling to nonlinear problems, such as damage or plasticity.

p0285 In sum, it is clear that peridynamics is currently in its infancy in describing the full complexity of the degradation mechanisms that can initiate and develop in laminated composites. Much progress is needed on how to control anisotropic failure and on how to introduce plasticity and time-dependent behaviors that will be crucial in describing impact-induced damage in composites. Yet, it seems clear that peridynamics will be able to overcome some recurrent limitations of classical continuum mechanics, because its raw mathematical formulation allows for the development of discontinuities. Future work is needed to make this theoretical tool fully applicable.

s0035 Acknowledgments

p0290 We acknowledge KAUST for funding part of this research and for providing the necessary technical support. Sandia National Laboratories is a multiprogram laboratory managed and operated by Sandia Corporation, a wholly owned subsidiary of

Comp. by: KKalaiselvi Stage: Proof Chapter No.: 12 Title Name: Camanho
Date:23/4/15 Time:13:19:29 Page Number: 349

To protect the rights of the author(s) and publisher we inform you that this PDF is an uncorrected proof for internal business use only by the author(s), editor(s), reviewer(s), Elsevier and typesetter SPi. It is not allowed to publish this proof online or in print. This proof copy is the copyright property of the publisher and is confidential until formal publication.

Lockheed Martin Corporation, for the U.S. Department of Energy's National Nuclear Security Administration under Contract DE-AC04-94AL85000.

References

Allix, O., Deu, J.F., 1997. Delayed-damage modelling for fracture prediction of laminated composites under dynamic loading. Eng. Trans. 45, 29–46.

Allix, O., Feissel, P., Thévenet, P., 2003. A delay damage mesomodel of laminates under dynamic loading: basic aspects and identification issues. Comput. Struct. 81, 1177–1191.

Allix, O., Ladevèze, P., 1995. Damage analysis of interlaminar fracture specimens. Compos. Struct. 31, 61–74.

Arnold, D.N., Brezzi, F., Cockburn, B., Marini, L.D., 2002. Unified analysis of discontinuous Galerkin methods for elliptic problems. SIAM J. Numer. Anal. 39, 1749–1779.

Askari, E., Xu, J., Silling, S.A., 2006. Peridynamic analysis of damage and failure in composites. In: 44th AIAA Aerospace Sciences Meeting and Exhibit, AIAA 2006-88.

Azdoud, Y., Han, F., Lubineau, G., 2013. A morphing framework to couple non-local to local anisotropic continua. Int. J. Solids Struct. 50, 1332–1341.

Azdoud, Y., Han, F., Lubineau, G., 2014. The morphing method as a flexible tool for adaptive local/non-local simulation of static fracture. Comput. Mech. 54, 711–722.

Barut, A., Madenci, E., Phan, N., 2014. Peridynamics damage prediction in composites due to compression after impact. In: 55th AIAA/ASMe/ASCE/AHS/SC Structures, Structural Dynamics, and Materials Conference, AIAA 2014-1525.

Breitenfeld, M.S., Geubelle, P.H., Weckner, O., Silling, S.A., 2014. Non-ordinary state-based peridynamic analysis of stationary crack problems. Comput. Methods Appl. Mech. Eng. 272, 233–250.

Chen, X., Gunzburger, M., 2011. Continuous and discontinuous finite element methods for a peridynamics model of mechanics. Comput. Methods Appl. Mech. Eng. 200, 1237–1250.

Colavito, K.W., Barut, A., Madenci, E., Phan, N., 2013. Residual strength of composite laminates with a hole by using peridynamic theory. In: 54th AIAA/ASME/ASCE/AHS/ASC Structures, Structural Dynamics, and Materials Conference, AIAA 2013-1761.

Han, F., Lubineau, G., 2012. Coupling of nonlocal and local continuum models by the Arlequin approach. Int. J. Numer. Methods Eng. 89, 671–685.

Hashin, Z., 1980. Failure criteria for unidirectional fiber composites. J. Appl. Mech. 47, 329–334.

Hinton, M.J., Kaddour, A.S., Soden, P.D., 2002. A comparison of the predictive capabilities of current failure theories for composite laminates, judged against experimental evidence. Compos. Sci. Technol. 62, 1725–1797.

Hu, W., Ha, Y.D., Bobaru, F., 2011. Modeling dynamic fracture and damage in a fiber-reinforced composite lamina with peridynamics. Int. J. Multiscale Comput. Eng. 9, 707–726.

Hu, W., Ha, Y.D., Bobaru, F., 2012. Peridynamic model for dynamic fracture in unidirectional fiber-reinforced composites. Comput. Methods Appl. Mech. Eng. 217, 247–261.

Hu, Y.L., Yu, Y., Wang, H., 2014. Peridynamic analytical method for progressive damage in notched composite laminates. Compos. Struct. 108, 801–810.

Jones, R.M., 1999. Mechanics of Composite Materials, second ed Brunner-Routledge, New York.

Comp. by: KKalaiselvi Stage: Proof Chapter No.: 12 Title Name: Camanho
Date:23/4/15 Time:13:19:29 Page Number: 350

To protect the rights of the author(s) and publisher we inform you that this PDF is an uncorrected proof for internal business use only by the author(s), editor(s), reviewer(s), Elsevier and typesetter SPi. It is not allowed to publish this proof online or in print. This proof copy is the copyright property of the publisher and is confidential until formal publication.

B978-0-08-100332-9.00012-8, 00012

Kilic, B., Agwai, A., Madenci, E., 2009. Peridynamic theory for progressive damage prediction in center-cracked composite laminates. Compos. Struct. 90, 141–151.

Kunin, I.A., 1983. Elastic Media with Microstructure II: Three-Dimensional Models. Springer-Verlag, Berlin.

Ladevèze, P., Le Dantec, E., 1992. Damage modeling of the elementary ply for laminated composites. Compos. Sci. Technol. 43, 257–267.

Ladevèze, P., Lubineau, G., 2001. On a damage mesomodel for laminates: micro-meso relationships, possibilities and limits. Compos. Sci. Technol. 61, 2149–2158.

Ladevèze, P., Lubineau, G., 2003. On a damage mesomodel for laminates: micromechanics basis and improvement. Mech. Mater. 35 (8), 763–775.

Ladevèze, P., Lubineau, G., Marsal, D., 2006. Towards a bridge between the micro- and the mesomechanics of delamination for laminated composites. Compos. Sci. Technol. 66 (6), 698–712.

Littlewood, D.J., 2010. Simulation of dynamic fracture using peridynamics, finite element modeling, and contact. In: ASME 2010 International Mechanical Engineering Congress and Exposition, pp. 209–217.

Liu, D., Jia, T., 2012. Peridynamic applications for orthotropic materials. Michigan State University, Final report.

Lubineau, G., Azdoud, Y., Han, F., Rey, C., Askari, A., 2012. A morphing strategy to couple non-local to local continuum mechanics. J. Mech. Phys. Solids 60, 1088–1102.

Lubineau, G., Ladevèze, P., 2008. Construction of a micromechanics-based intralaminar mesomodel, and illustrations in ABAQUS/standard. Comput. Mater. Sci. 43, 137–145.

Madenci, E., Oterkus, E., 2014. Peridynamic Theory and its Applications. Springer, New York.

Oterkus, E., 2010. Peridynamic theory for modeling three-dimensional damage growth in metallic and composite structures. Ph.D. thesis. University of Arizona.

Oterkus, E., Madenci, E., Weckner, O., Silling, S., Bogert, P., Tessler, A., 2012. Combined finite element and peridynamic analyses for predicting failure in a stiffened composite curved panel with a central slot. Compos. Struct. 94, 839–850.

Oterkus, S., Madenci, E., 2014. Fully coupled thermomechanical analysis of fiber reinforced composites using peridynamics. In: 55th AIAA/ASMe/ASCE/AHS/SC Structures, Structural Dynamics, and Materials Conference, AIAA 2014-0694.

Seleson, P., Beneddine, S., Prudhomme, S., 2013. A force-based coupling scheme for peridynamics and classical elasticity. Comput. Mater. Sci. 66, 34–49.

Silling, S.A., 2000. Reformulation of elasticity theory for discontinuities and long-range forces. J. Mech. Phys. Solids 48, 175–209.

Silling, S.A., 2010. Linearized theory of peridynamic states. J. Elast. 99, 85–111.

Silling, S.A., 2014. Origin and effect of nonlocality in a composite. J. Mech. Mater. Struct. 9, 245–258.

Silling, S.A., Askari, E., 2005. A meshfree method based on the peridynamic model of solid mechanics. Comput. Struct. 83, 1526–1535.

Silling, S.A., Lehoucq, R.B., 2010. Peridynamic theory of solid mechanics. Adv. Appl. Mech. 44, 73–168.

Silling, S.A., Epton, M., Weckner, O., Xu, J., Askari, E., 2007. Peridynamic states and constitutive modeling. J. Elast. 88, 151–184.

Soden, P.D., Hinton, M.J., Kaddour, A.S., 1998. A comparison of the predictive capabilities of current failure theories for composite laminates. Compos. Sci. Technol. 58, 1225–1254.

Tupek, M.R., Radovitzky, R., 2014. An extended constitutive correspondence formulation of peridynamics based on nonlinear bond-strain measures. J. Mech. Phys. Solids 65, 82–92.

Comp. by: KKalaiselvi Stage: Proof Chapter No.: 12 Title Name: Camanho
Date:23/4/15 Time:13:19:29 Page Number: 351

To protect the rights of the author(s) and publisher we inform you that this PDF is an uncorrected proof for internal business use only by the author(s), editor(s), reviewer(s), Elsevier and typesetter SPi. It is not allowed to publish this proof online or in print. This proof copy is the copyright property of the publisher and is confidential until formal publication.

B978-0-08-100332-9.00012-8, 00012

Tupek, M.R., Rimoli, J.J., Radovitzky, R., 2013. An approach for incorporating classical continuum damage models in state-based peridynamics. Comput. Methods Appl. Mech. Eng. 263, 20–26.

Xu, J., Askari, A., Weckner, O., Razi, H., Silling, S., 2007. Damage and failure analysis of composite laminates under biaxial loads. In: 48th AIAA Structures, Structural Dynamics, and Materials Conference, AIAA 2007-2315.

Xu, J., Askari, A., Weckner, O., Silling, S., 2008. Peridynamic analysis of impact damage in composite laminates. J. Aerosp. Eng. 21, 187–194.

Comp. by: KKalaiselvi Stage: Proof Chapter No.: 12 Title Name: Camanho
Date:23/4/15 Time:13:19:29 Page Number: 352

To protect the rights of the author(s) and publisher we inform you that this PDF is an uncorrected proof for internal business use only by the author(s), editor(s), reviewer(s), Elsevier and typesetter SPi. It is not allowed to publish this proof online or in print. This proof copy is the copyright property of the publisher and is confidential until formal publication.

Non-Print Items

Abstract

Peridynamics has been recently introduced as a way to simulate the initiation and propagation of multiple discontinuities (e.g., cracks). It is an alternative to classical continuum damage mechanics and fracture mechanics and is based on a nonlocal rewriting of the equilibrium equation. This new technique is particularly promising in the case of composite materials, in which very complex mechanisms of degradation must be described. We present here some fundamental aspects of peridynamics models for composite materials, and especially laminates. We also propose an approach to couple peridynamics domains with classical continuum mechanics (which relies on the concept of contact forces) by the use of a recently introduced coupling technique: the morphing technique, that appears to be a very versatile and powerful tool for coupling local to nonlocal descriptions.

Keywords: Composites, Peridynamics, Coupling, Morphing technique.